JOC The Journal of Organic Chemistry

Article

pubs.acs.org/joc

Insight into and Computational Studies of the Selective Synthesis of 6*H*-Dibenzo[*b*,*h*]xanthenes

Paula F. Carneiro,[†] Maria do Carmo F. R. Pinto,[†] Roberta K. F. Marra,[‡] Vinícius R. Campos,[‡] Jackson Antônio L. C. Resende,[‡] Maicon Delarmelina,[‡] José Walkimar M. Carneiro,[‡] Emerson S. Lima,[§] Fernando de C. da Silva,[‡] and Vitor F. Ferreira*[,‡]

[†]Universidade Federal do Rio de Janeiro, Instituto de Pesquisas de Produtos Naturais, 21944-970 Rio de Janeiro, RJ, Brazil

[‡]Universidade Federal Fluminense, Instituto de Química, 24020-150 Niterói, RJ, Brazil

[§]Universidade Federal do Amazonas, Faculdade de Ciências da Saúde, 69010-300 Manaus, AM, Brazil

Supporting Information

ABSTRACT: Starting from 2-hydroxy-1,4-naphthoquinone (lawsone), we synthesized eight new 6*H*-dibenzo[*b*,*h*]xanthene derivatives selectively under solvent-free conditions. Spectroscopic investigations confirmed that only the isomer 6*H*-dibenzo[*b*,*h*]xanthene was obtained in all eight cases. Computational studies provide a rationalization for the selective appearance of these isomers having as an intermediate an addition product.

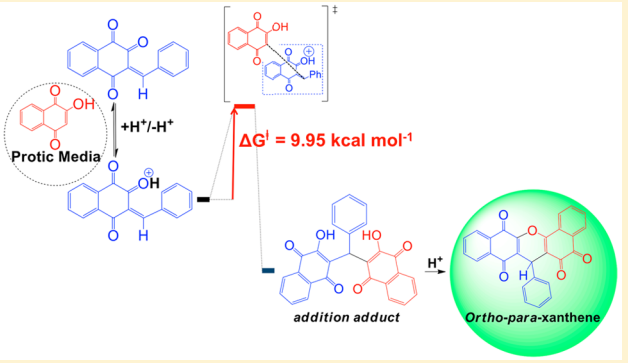

INTRODUCTION

9*H*-Xanthene [**1** (Figure 1)] is a general class of natural and synthetic heterocyclic compounds[1−3] with many biological applications in addition to functionality as fluorescent dyes.[4] In the biological field, these heterocyclic compounds exhibit a broad spectrum of activities, including trypanothione reductase inhibiting,[5] antiviral,[6] antibacterial,[7,8] antiplasmodial,[9,10] antimalarial,[11] antifungal,[12] anti-inflammatory,[13] anticancer,[14−17] and antihypertensive[18] activity, and are used in photodynamic therapy.[19] Because of their biological properties, 9*H*-xanthene derivatives have been prepared by several procedures.[20−23]

The biological activity of quinones[24] against several biological targets has shown that the activities of these molecules are due to their ability to accept one or two electrons in the so-called redox cycle to form an anion or dianion *in situ* that is known as a reactive oxygen species (ROS).[25,26] Thus, the semiquinone radicals can improve the conditions for intracellular hypoxia by producing superoxide anions.[27−30] Through this mechanism, quinones are cytotoxic to both normal and tumor cells in mammals as well as to various microorganisms, ultimately leading to programmed cell death (apoptosis).[31,32]

Several procedures have been described for the preparation of type **1** xanthenes (Figure 1), most of them based on a two- or three-component reaction of *β*-naphthol with aldehydes.[33−44] When naphthoquinones are fused to the xanthenes, two subclasses of products might be produced, which have also been prepared by several synthetic methods (Figure 1): benzoxanthenes with one naphthoquinone moiety, represented by compound **2** and its isomer **3** and compound **4** and its isomer **5**,[45−52] and dibenzoxanthenes with two naphthoquinone moieties attached to the central pyran ring, which can have three possible isomers, **6**−**8**. Tisseh et al.[53] were the first to report a simple and efficient method for the preparation of dibenzoxanthene derivatives under solvent-free conditions (10 mol % *p*-toluenesulfonic acid), which they assumed to be the [*b*,*i*] isomers, but the products suffered from very poor spectroscopic characterization.[53] The ^{1}H NMR (DMSO-d_6) spectrum for **6** (Ar = Ph) reported all the aromatic signals as one broad signal, δ 7.16−8.08 (13H). After this publication, further studies referred to these results and reported the same symmetrical structure **6**.[44,54−62] Despite the several methods described in the literature for preparing dibenzoxanthene **6** (dibenzo[*b*,*i*]xanthene), the corresponding synthesis of dibenzoxanthenes of types **7** (dibenzo[*b*,*h*]xanthene) and **8** (dibenzo[*c*,*h*]xanthene) has not yet been reported.

According to the literature, the formation of dibenzoxanthenes starts by the addition of lawsone to the appropriate aldehydes, yielding an intermediate *o*-quinone methide that reacts further with another molecule of lawsone to afford corresponding open adduct **9**,[63] which upon cyclization can form isomeric compounds **6**−**8**. Mathieson and Thomson described the formation of three possible isomers when they attempted to cyclize an open ring adduct of lawsone and

Received: April 17, 2016
Published: June 9, 2016

DOI: 10.1021/acs.joc.6b00864
J. Org. Chem. 2016, 81, 5525−5537

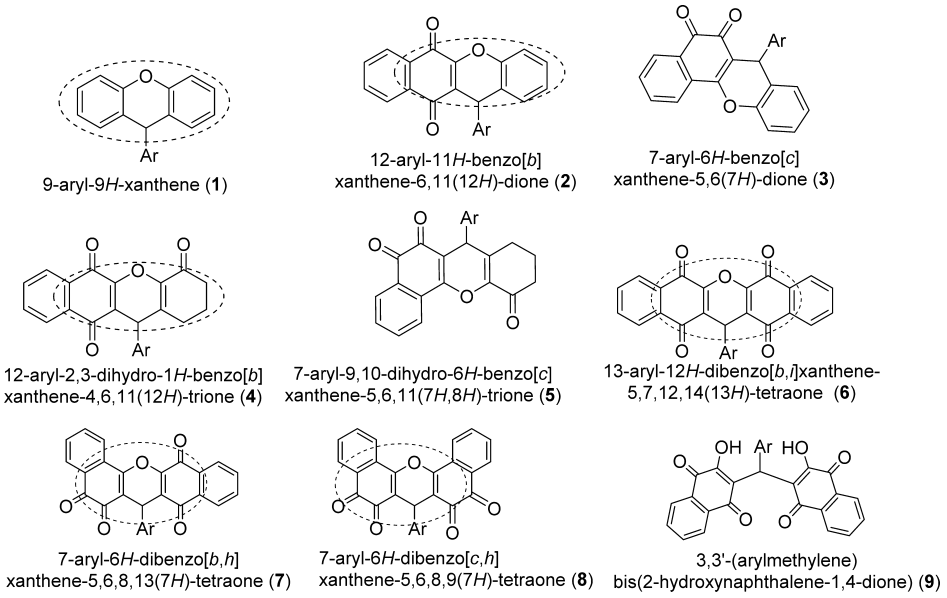

Figure 1. General structures of xanthenes, benzoxanthenes, and dibenzoxanthenes.

acetaldehyde.[64] On the basis of the observation of three carbonyl bands in the infrared spectrum, they believed that they obtained dibenzoxanthene type **7**. Since then, most of the reports in the literature describe the reactions of lawsone and aldehydes[65] under acidic catalysis with and without solvents form exclusively or in high yields dibenzo[*b*,*i*]xanthene isomers of type **6**.

In this work, we study a series of reaction conditions in the hopes of optimizing the formation of each of these dibenzoxanthene isomers.

RESULTS AND DISCUSSION

Reactions for preparing benzoxanthenes of type **6** (*para-para* isomer) have been reported in solvents using acid catalysis with solvents or under solvent-free conditions. Our synthetic study toward compounds **6** was initiated by reacting lawsone with benzaldehyde in an ethanol/water solvent (1:1) under reflux (Scheme 1). It was observed that the reaction led to the formation of a yellow precipitate in the reaction flask that was filtered and stored in a desiccator with phosphorus pentoxide to remove the residual water. The solid was obtained in 83% yield, and its structure was elucidated by spectroscopic techniques.

Scheme 1. General Synthetic Routes Used in This Study

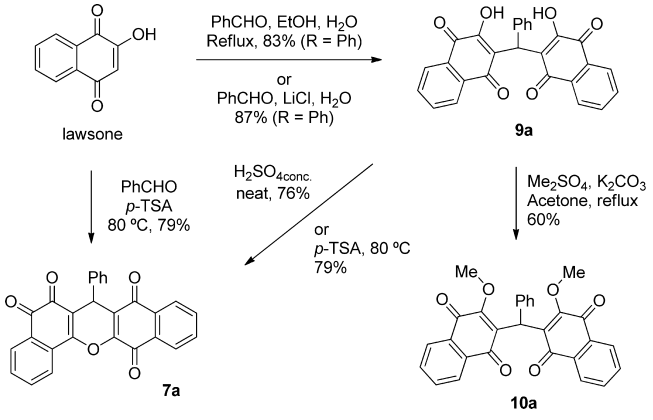

Hydroxyl bands were observed in the infrared spectra, indicating that the structure is the open bis(2-hydroxynaphthalene-1,4-dione) (**9a**, where R = Ph). To confirm the structures of the compound, a reaction described by Tisseh and Bazgir[66] was performed by conducting the same reaction in the presence of a catalytic amount of LiCl in aqueous media. The same compound **9a** was obtained in 87% yield. Our product was compared with the one obtained in ref 66: mp 201 (lit. 202−204 °C); hydroxyl and carbonyl bands in the IR spectrum at 3335 (lit. 3332 cm^{-1}) and 1641 (lit. 1669 cm^{-1}); and a methine proton at δ 6.25 (lit. δ 6.00). Despite little difference between the carbonyl (C-1 and C-4) absorption bands in the infrared spectrum of **9a**, the ^{1}H NMR spectrum shows the structure is symmetrical. All these data indicate that compound **9a** was obtained in the reactions in both ethanol/water (1:1) and water/LiCl solvents. Additionally, compound **9a** was fully methylated by treatment with Me_2SO_4/K_2CO_3, producing compound **10a** (Scheme 1).

Because there are several reports showing that this reaction can be performed without solvent, producing compounds of type **6** in good yields, we decided to perform the reaction of lawsone with benzaldehyde in the presence of a catalytic amount of *p*-toluenesulfonic acid at 80 °C. These are the same conditions used by Bazgir et al.[62] The solid ground mixture was heated in a preheated oven for 6−7 h, and a deep red product was isolated in 79% yield.

The IR spectra of the red product did not indicate the presence of a hydroxyl group as in compound **9a**, and its mp (277−280 °C) was much lower than those of the isomers of type **6** (R^1, R^2, R^3 = H; 305−307 °C[53,62]) reported in the literature. The ^{1}H NMR and ^{1}H−^{1}H COSY spectra in $CDCl_3$ of the product were quite different from the data reported for compounds of type **6**, showing three sets of signals: *p*-quinone, *o*-quinone, and phenyl ring. These unsymmetrical signals of the aromatic region also eliminate the possibility of the red compound being an isomer of type **8** (*ortho-ortho*). The methine proton (H-7) in ^{1}H NMR was at δ 5.37, lower than that of **9a** (δ 6.25) and higher than that of **6** (δ 5.09[53,62]). Similarly, the ^{13}C NMR showed many more signals than expected for a symmetrical structure like **6** and two different

DOI: 10.1021/acs.joc.6b00864
J. Org. Chem. 2016, 81, 5525−5537

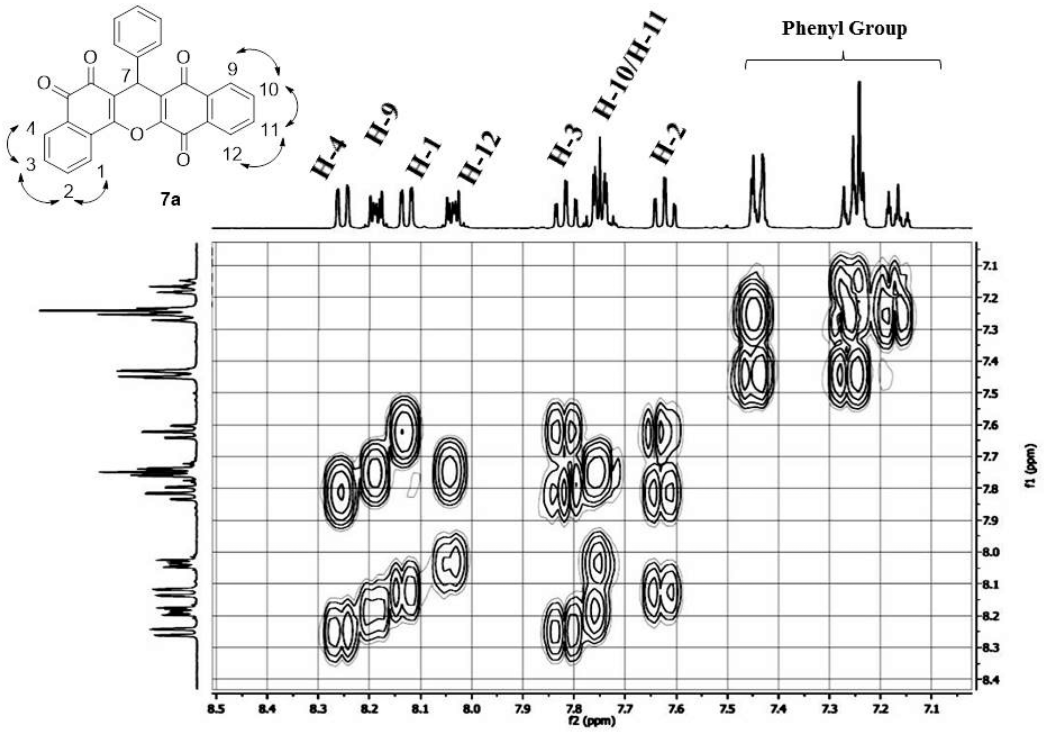

Figure 2. $^{1}H-^{1}H$ correlation spectroscopy of **7a** in $CDCl_3$.

signals at δ 156.1 and 148.5 for the sp^2 carbons bonded to the oxygen of the pyran ring. The complete and unambiguous assignment of hydrogens for structure **7a** was based on the analysis of the multiplicity patterns of proton resonances and also on the use of a homonuclear $^{1}H-^{1}H$ COSY spectrum (Figure 2) that showed all the hydrogens correlated to the *ortho-para* quinone. We described the hydrogens of the *o*-quinone side as δ 8.14 (dd, J = 7.8 and 1.0 Hz, 1H, H-1), 7.63 (dt, J = 7.8 and 1.0 Hz, 1H, H-2), 7.83 (dt, J = 7.8 and 1.0 Hz, 1H, H-3), and 8.27 (dd, J = 7.8 and 1.0 Hz, 1H, H-4). For the *p*-quinone side, we observed hydrogens at δ 7.74–7.79 (m, 2H, H-10 and H-11), 8.04–8.06 (m, 1H, H-12), and 8.19–8.21 (m, 1H, H-9).

To confirm the structure of **7a**, we decided to prepare an *o*-phenylenediamine derivative (Scheme 2). This reagent reacts only via its *o*-quinone moiety. Adduct **11a** was obtained in good yield and recrystallized in a mix of hexane and dichloromethane, providing suitable crystals for the X-ray crystallography study. The structure of substance **11a** was confirmed by X-ray diffraction (Figure 3), which confirms the pattern of *o*- and *p*-naphthoquinone for **7a**. The phenyl ring is oriented nearly perpendicular to the ring plane in benzoxanthenes.

Scheme 2. Phenazine 11a Derivative from *o*- and *p*-Naphthoquinone for 7a

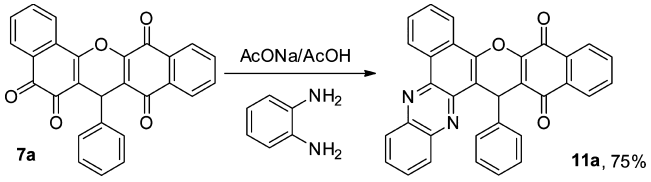

The reaction between lawsone and other aldehydes was tested for eight examples, and the produced 6*H*-dibenzo[*b*,*h*]-xanthenes **7a–h** were obtained in high yields (Scheme 3). Depending on the reactivity of the aldehyde, the reaction takes 6–7 h to complete. Liquid aldehydes at 80 °C reacted quickly. For the best performance of this methodology, the temperature must be approximately 80 °C, because if the temperature is increased to 100 °C, the yield decreases dramatically, and when the temperature exceeds 120 °C, there is complete degradation of the starting material and the product. An example of this is the fact that substance **7h** at 80 °C has a yield of 72% while at 100 °C has a yield of 19%, and above 120 °C, it is not possible to isolate the product. All compounds had the same spectroscopic characteristics as derivative **7a** (see the Supporting Information).

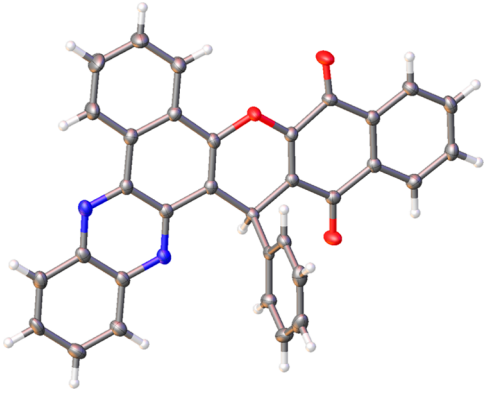

Figure 3. ORTEP diagram of compound **11a** showing 50% probability ellipsoids. Hydrogen, carbon, nitrogen, and oxygen atoms are colored white, gray, blue, and red, respectively.

To test if compound **9a** is the intermediate for **7a**, we attempted to cyclize it under several conditions such as with H_2SO_4 (concentrated) and *p*-toluenesulfonic acid without

DOI: 10.1021/acs.joc.6b00864
J. Org. Chem. 2016, 81, 5525–5537

Scheme 3. Optimized Conditions for Preparing 6*H*-Dibenzo[*b*,*h*]xanthenes (7a–h)

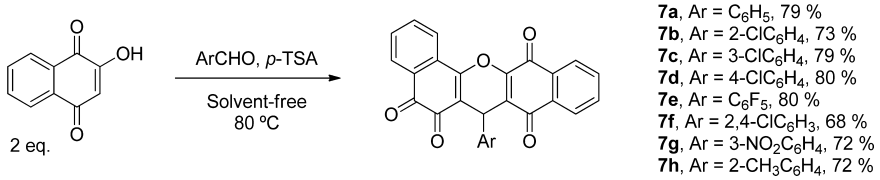

Scheme 4. Quinone Methide Formation in a Protic Medium

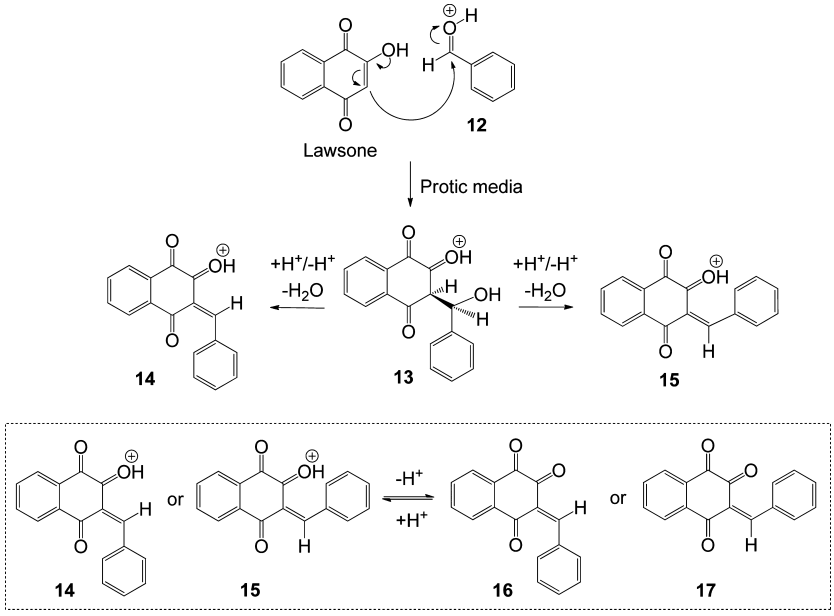

solvent (80 °C). In all cases, the 6*H*-dibenzo[*b*,*h*]xanthene (**7a**) was formed.

These data contradict what is reported in the literature.[53,62,66] Therefore, we decided to conduct a computational study to understand the mechanism involved in this reaction and further corroborate the results.

The xanthene derivatives can be obtained after the *in situ* formation of the quinone methide and the subsequent cycloaddition reaction with a second lawsone molecule.[67] A proposed mechanism for the quinone methide formation in a protic medium is shown in Scheme 4. After the nucleophilic attack of lawsone on protonated aldehyde **12**, followed by water elimination, quinone methides **16** and **17** may be formed by protonation/deprotonation in an acid–base equilibrium.

The reaction mixture can be described as a protic medium even when an aprotic solvent is used, as lawsone itself has some acidic character and may dissociate into lawsonate and hydronium ions in the presence of a weak base.

Elimination of water from **13** affords the quinone methides as *E* isomers (**14**) or *Z* isomers (**15**). The dehydration process is not reversible, and an isomer interconversion equilibrium will not be observed during the subsequent cycloaddition reaction with lawsone. The computation of the relative stabilities of the two isomers shows that the *Z* isomer (**15** and **17**) is the most stable, but by less than 1.0 kcal mol^{-1} (see Table S1). Because of this small energy difference between the *E* and *Z* isomers, both were investigated in the following computations.

The next point we investigated was the reaction between the quinone methides and the second lawsone molecule, which may happen by either an addition reaction or an asynchronous cycloaddition. Because of the asymmetric nature of these molecules, at least 16 distinct transition structures for the reaction between lawsone and quinone methides **16** and **17** may be predicted, depending on the different arrangements for approximation between the two reactants [**18**–**25** (Figure 4)]. A clear picture emerges from preliminary gas phase calculations. When the lawsone approaches the quinone methides in an orientation where the carbon atom bearing the hydroxyl group of lawsone (C_2) forms a carbon–carbon bond with the substituted carbon atom (C_{11}) of the quinone methides [arrangements **18**, **20**, **23**, and **25** (Figure 4)], the relative activation energies of the corresponding transition structures are much higher than those computed when the approach occurs in the opposite way [structures **19**, **21**, **22**, and **24** (Figure 4)]. These results lead us to exclude these alternatives from the following discussion. Additionally, for all examples we computed, transition structures in an *endo* orientation have relative energies lower than those of the corresponding compounds in an *exo* orientation, although in these cases, the energy differences between two isomers differing only in the *endo* or *exo* orientation are much smaller.

Among the structures with an *endo* orientation, structures **19** and **22**, derived from the *E*- and *Z*-quinone methide isomers, respectively, have the lowest relative energies. Therefore, we considered these two isomers (**19** and **22**) to compute the activation Gibbs free energy and the reaction Gibbs free energy. In Figure 5, we provide results obtained from gas phase calculations (bold) as well as those obtained with the polarized continuum solvation model (IEFPCM) (in parentheses) using water as an implicit solvent.

All four arrangements lead to activation free energies ($\Delta G^{\ddagger}$) between 22 and 26 (20 and 23 in the solvent) kcal mol^{-1}, with

DOI: 10.1021/acs.joc.6b00864
J. Org. Chem. 2016, 81, 5525–5537

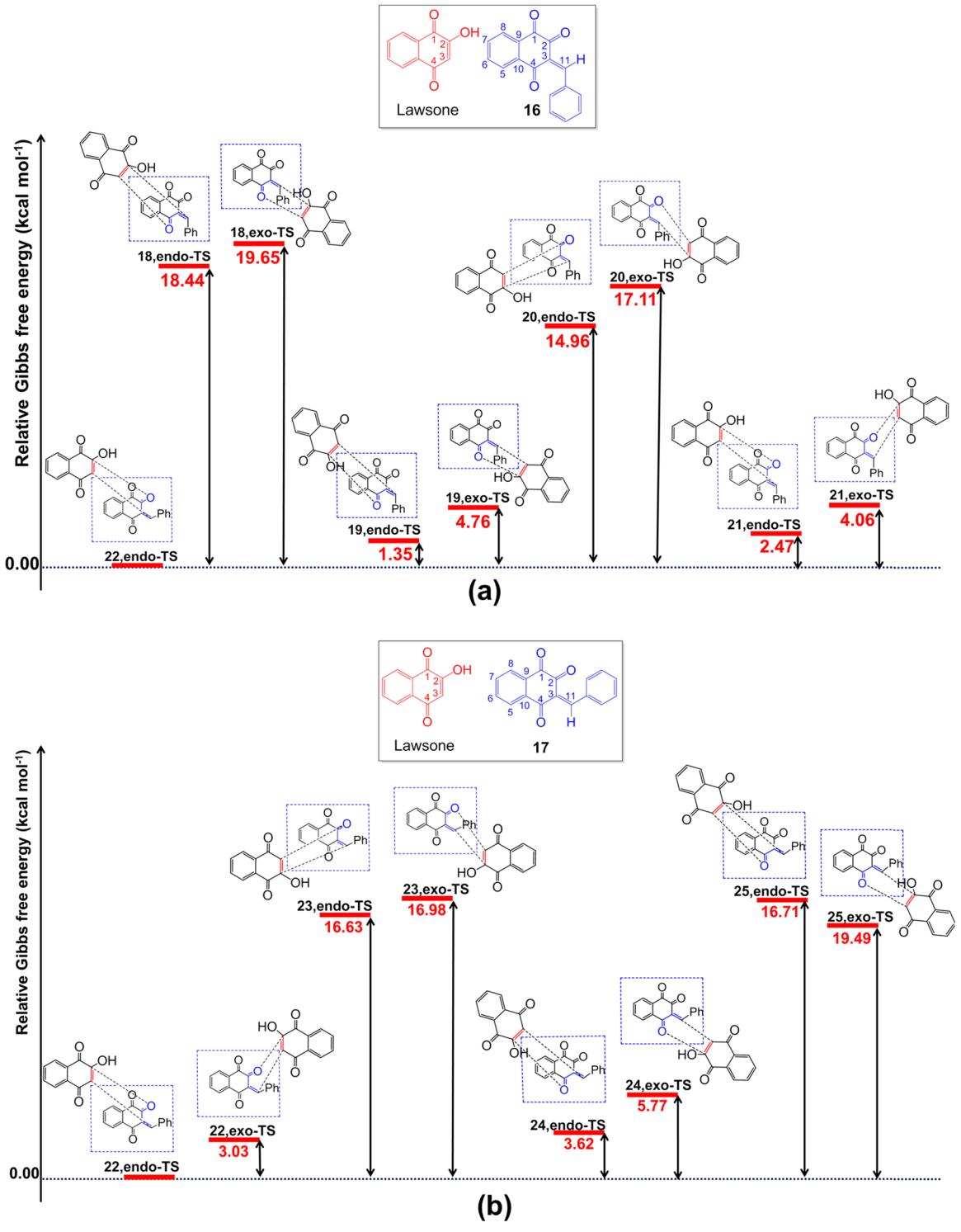

Figure 4. Gas phase relative Gibbs free energy for possible transition structures for the reaction between lawsone and the quinone methide (a) *E* isomer or (b) *Z* isomer. The values are the relative Gibbs free energies in kilocalories per mole, taking the **22**,endo-TS structure as the reference. Method: wb97xd/6-31+G(d,p).

the lowest value obtained for the **22**,endo case. Intrinsic reaction coordinate (IRC) calculations confirmed the connection between the reactants and corresponding intermediates **19** and **22**. As indicated, the cyclic intermediates result from a Diels−Alder type cycloaddition reaction, with the intermediate obtained from the **22**,endo approach being the most stable. Potential energy representations obtained from the IRC calculations are consistent with a one-step one-stage process for these reactions. The polar solvent water reduces the activation energy by 2−3 kcal mol^{-1} and leads to more polar transition structures typical of a two-stage process.

The transition structures have a high degree of asynchronicity. The formation of the C−C bond occurs in a much earlier stage than the formation of the C−O bond, resulting in much different C−C and C−O bond distances in the transition structures. Figure 6 shows the relevant distances for each

DOI: 10.1021/acs.joc.6b00864
J. Org. Chem. 2016, 81, 5525−5537

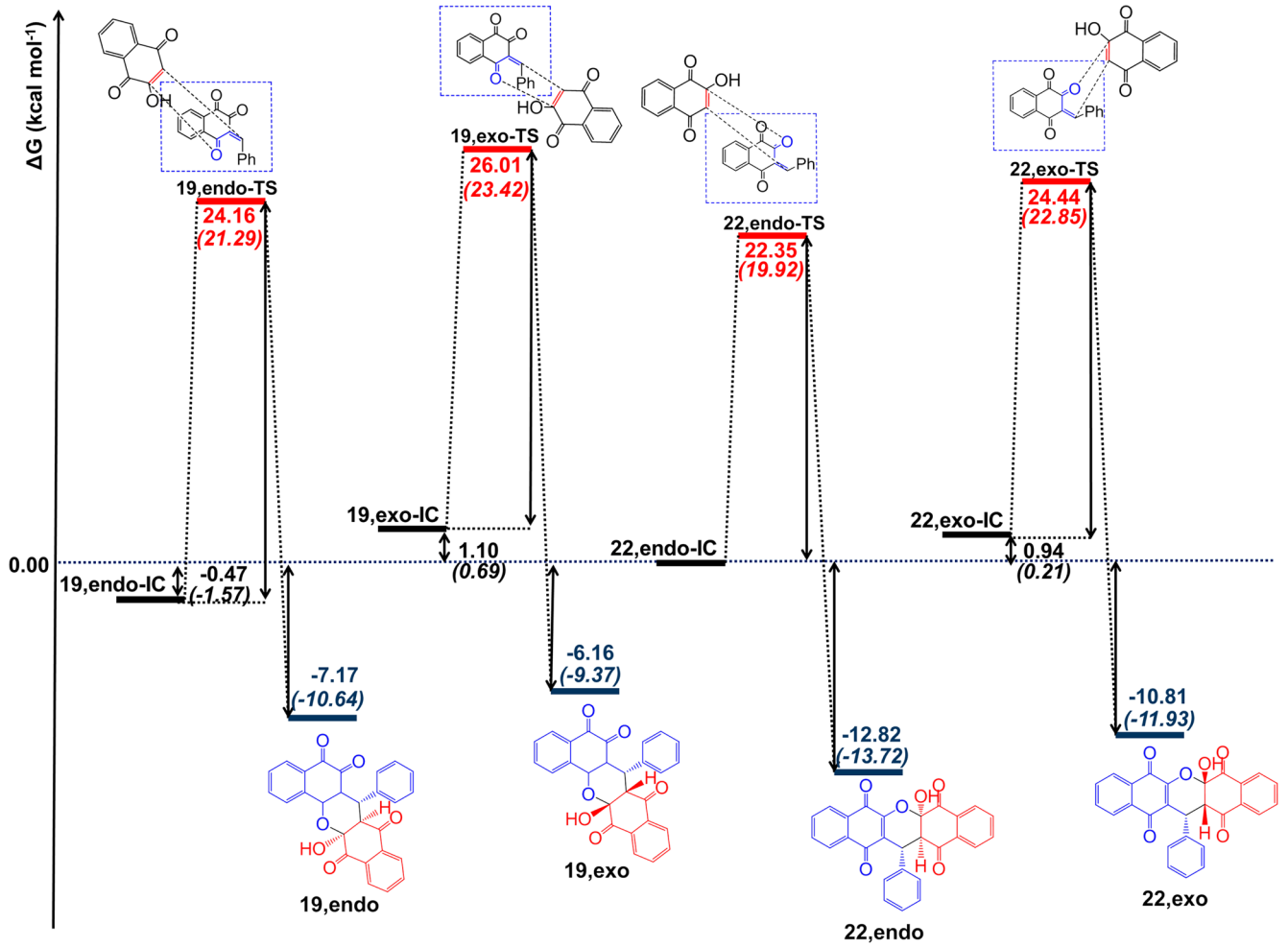

Figure 5. Activation and reaction Gibbs free energy for the reaction between quinone methides (**16** and **17**) and lawsone. Gas phase (bold) and IEFPCM (in parentheses; solvent, water) results are given. IC stands for initial complex, a stationary point formed by a loose complex between the two reactants. Values are given in kilocalories per mole relative to the energy of the **22**,endo-IC initial complex. Method: wb97xd/6-31+G(d,p).

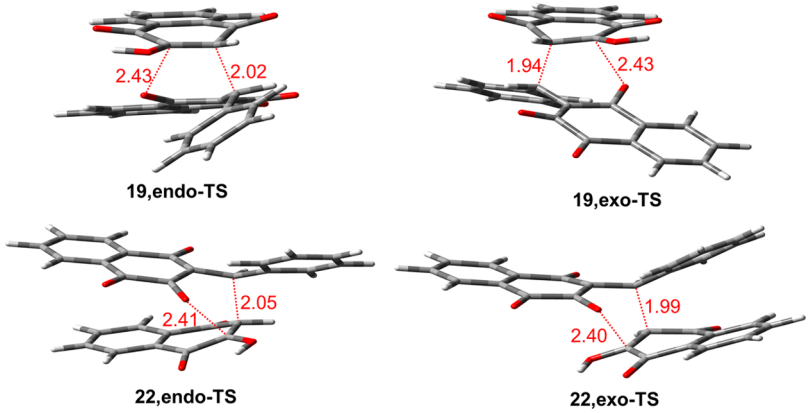

Figure 6. Transition state structures for the formation of intermediates **19** and **22** starting from deprotonated quinone methides **16** and **17**. Distances are in angstroms. Method: wb97xd/6-31+G(d,p).

isomer (**19** and **22**) obtained from geometry optimization in the gas phase. The C−C bond distances in the transition state range from 1.94 to 2.05 Å, while the C−O bond distances range from 2.43 to 2.45 Å.

An acid−base equilibrium is involved in the *in situ* formation of the quinone methides (see Scheme 3). As low activation energies are common in these prototropic equilibria, the protonated forms of the quinone methides (**14** and **15**) could compete with the deprotonated forms (**16** and **17**) and may also undergo addition/cycloaddition reaction in the presence of lawsone. To verify this hypothesis, we repeated all the calculations using the protonated forms of the quinone methides (**14** and **15**) in the **26**−**29** approach modes (Figure 7). As could be anticipated, the most basic site of the quinone

DOI: 10.1021/acs.joc.6b00864
J. Org. Chem. 2016, 81, 5525−5537

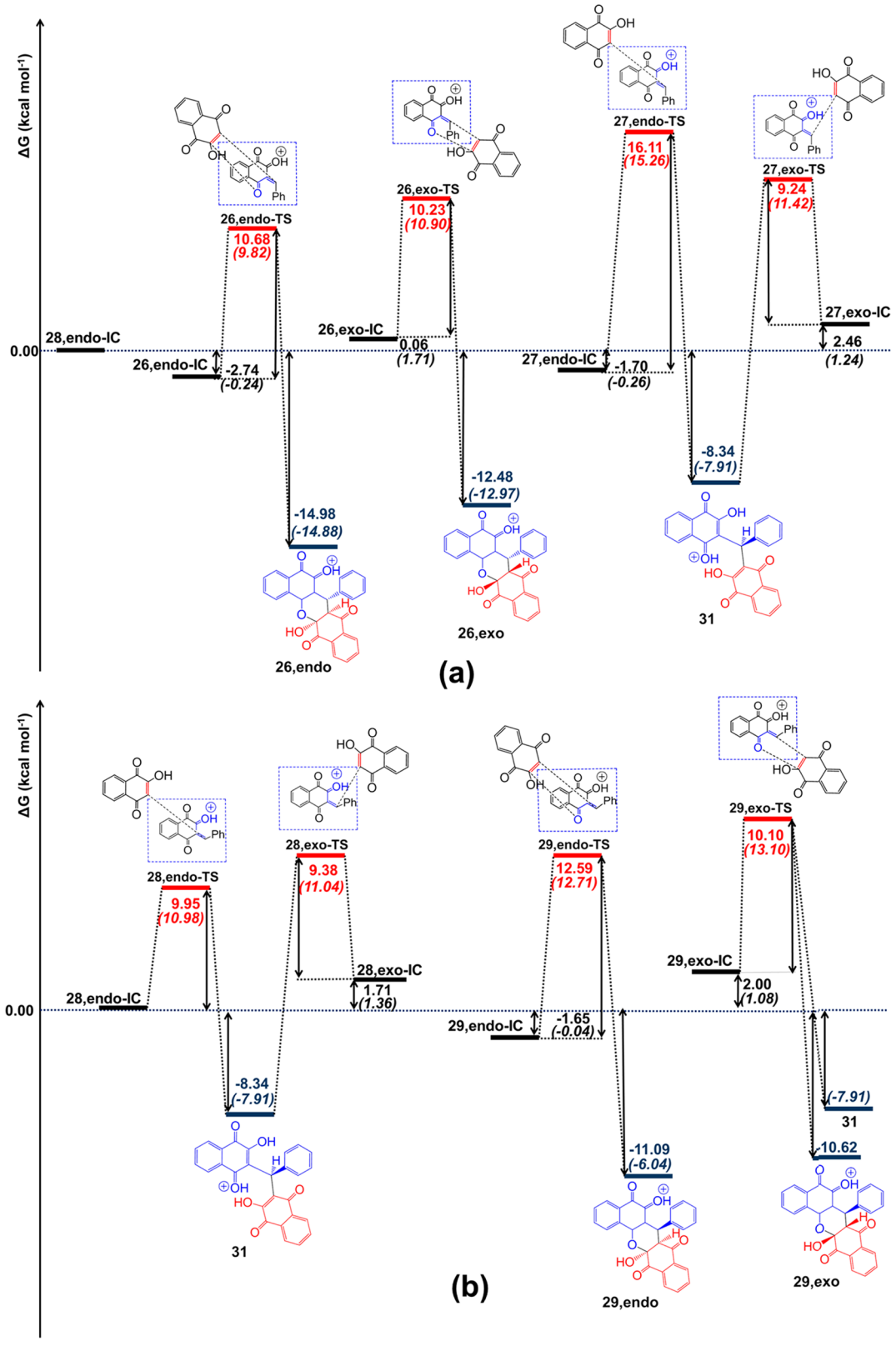

Figure 7. Relative activation and reaction Gibbs free energies for the reaction of protonated quinone methides [(a) **14** and (b) **15**] with lawsone. Gas phase (bold) and IEFPCM (in parentheses; solvent, water) results are given. All values are in kilocalories per mols and are given relative to the **28**,endo-IC initial complex. Method: wb97xd/6-31+G(d,p).

methides is the 1,2-quinone moiety, with the proton sitting between the two carboxyl groups. This is the form we adopted in all the calculations reported below. The $\Delta G^{\ddagger}$ values for the two possible mechanisms were compared.

The first point to which we call attention is the considerable decrease in the activation energy. The calculated $\Delta G^{\ddagger}$ values for the reaction using the protonated quinone methides (Figure 7) are 10−16 kcal mol^{-1} lower than the corresponding activation

DOI: 10.1021/acs.joc.6b00864
J. Org. Chem. 2016, 81, 5525−5537

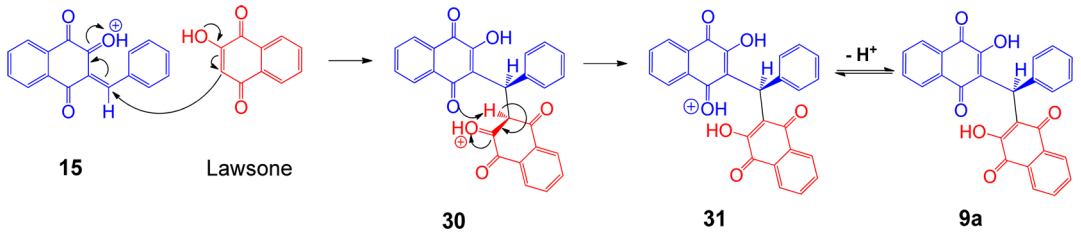

Figure 8. Formation of open adduct **9a**.

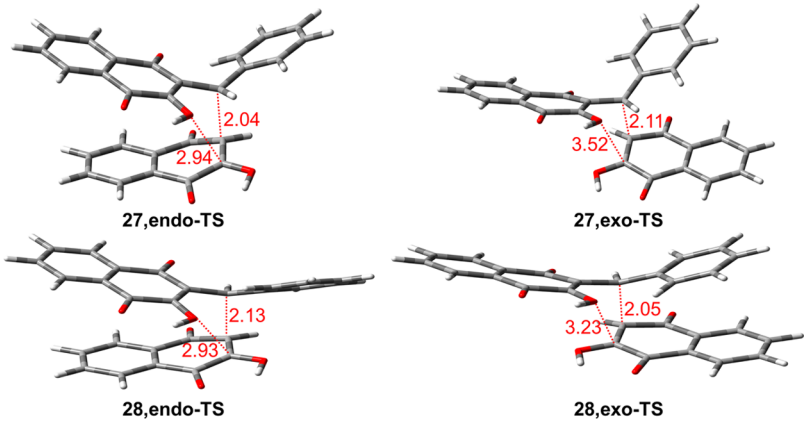

Figure 9. Transition structures for the **27** and **28** approach modes from the protonated quinone methide to lawsone. Bond distances are in angstroms. Method: wb97xd/6-31+G(d,p).

energies for the reaction using the deprotonated systems (Figure 5). Therefore, as the medium has at least the residual proton from the formation of the quinone methide (see Scheme 3), the most probable reaction pathway in the second step of the reaction surely involves one of the protonated forms of the quinone methides. Additionally, as the protonation of the 1,2-quinone moiety of the quinone methide increases the electrophilicity of C-11 (see the inset in Figure 4), the reaction becomes still more asynchronous than the corresponding reaction with the deprotonated form of the quinone methide, which, as mentioned above, is already considerably asynchronous. This introduces a new alternative to the reaction mechanism. For these highly asynchronous reactions, addition, instead of cycloaddition, may be observed, in line with the experimental findings. The relative activation energies provided in Figure 7 show that the cycloaddition reaction is not always the less energetic process for the reaction of a protonated quinone methide with lawsone. Therefore, the acid−base equilibrium involving the protonated forms of the quinone methides (**14** and **15**) provides a second pathway for the reaction.

As indicated in Figure 7, the nucleophilic approach of lawsone to the protonated quinone methide (arrangements **27** and **28**) might lead to addition adduct **31**, with an activation energy that is at least competitive with that of the cycloaddition process. Indeed, the lowest activation energy overall was found for the formation of addition adduct **31**. Depending on the orientation of some C−H bonds, the optimization of **30** (Figure 8) results in intramolecular hydrogen transfer to directly give open species **31** and **9a**, which are the same species that were experimentally characterized. Of course, a similar hydrogen transfer may also be facilitated by any base present in the reaction mixture. Transition structures to form a direct Diels−Alder intermediate could be located only when approaching the lawsone on the deprotonated moiety of the quinone methide, although with activation energies that are of the same order of magnitude or higher than those of the corresponding reaction for the formation of the addition adduct.

The orientation of the phenyl group of the quinone methide seems to have an important role in product formation when the lawsone nucleophile approaches the quinone methide. The approximation of the lawsone over the phenyl ring of the *Z* isomer (**15**) resulted in the less energetic pathway (**28**) and produced open adduct **31**. The *ortho-para* cycloaddition (**26**,endo) product was obtained when the lawsone nucleophile approached over the phenyl group of the *E* isomer (**14**).

The quinone methides are electron-poor dienes. In the presence of an electron-rich dienophile, they may undergo an inverse electron demand Diels−Alder reaction.[68] The electrophilicity of the diene is increased by the electron-withdrawing effect when the 1,2-quinone moiety of the quinone methide is protonated, strengthening the polar interaction due to charge transfer from the dienophile to the diene, with a corresponding decrease in the activation energy barrier.[69,70] A low distortion energy also contributes to the reduced activation free energy, as a highly polar Diels−Alder mechanism demands a lower reactant distortion to form the transition state.[71]

For the systems studied in this work, highly asynchronous transition states were observed, changing from a concerted one-stage mechanism to a two-stage [**26** and **29** (Figure 7)] or stepwise [**27** and **28** (Figure 7)] pathway. The latter is an extreme case in which addition, with the formation of an open adduct, instead of cyclization, is the main pathway. The strong ability of the protonated diene to stabilize the increasing electronic density due to the addition process resulted in a stable intermediate that did not proceed further to cyclization.[72] Therefore, the whole spectrum of possible alternatives may be

DOI: 10.1021/acs.joc.6b00864
J. Org. Chem. 2016, 81, 5525−5537

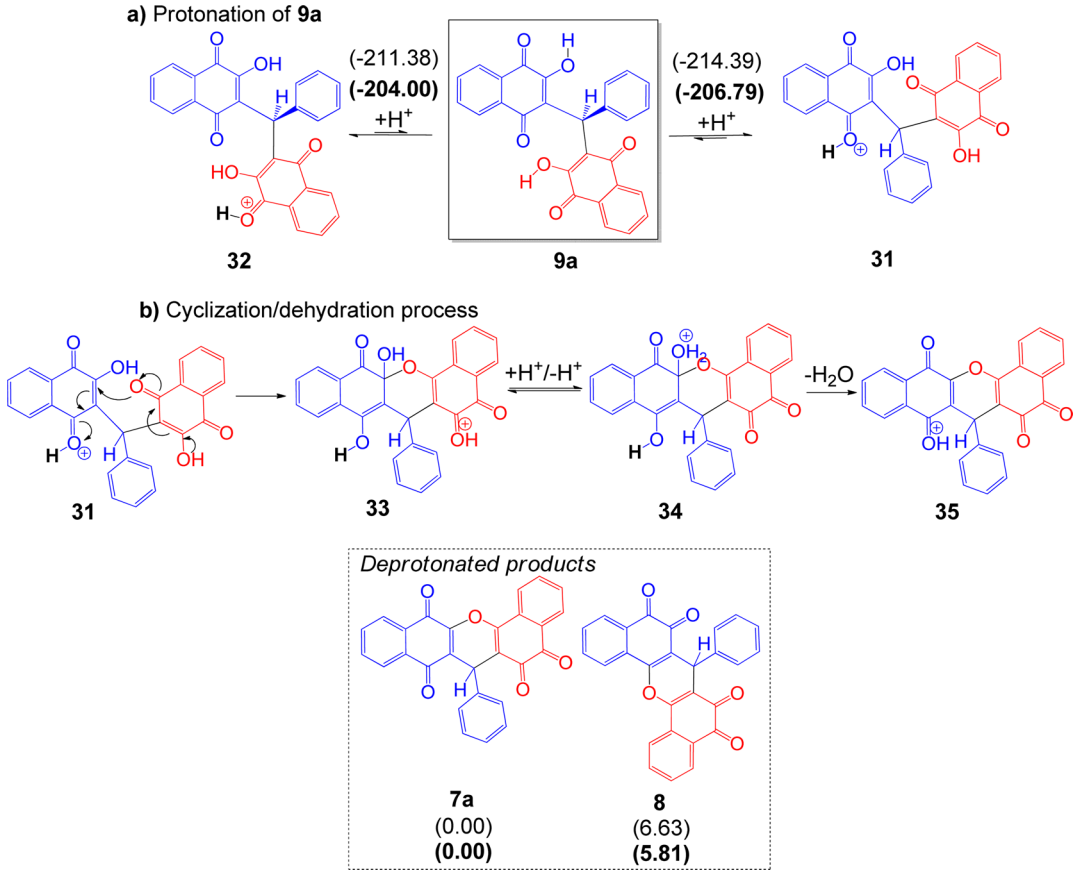

Figure 10. Enthalpy (plain in parentheses) and Gibbs free energy (bold in parentheses) changes for the protonation of open adduct **9** (a). Proposed cyclization mechanism for **31** in acidic media and relative enthalpy (plain) and Gibbs free energy (bold) of *para-ortho* **7a** and *ortho-ortho*-xanthene **8** derivatives (b). All values are in kilocalories per mole. Method: wb97xd/6-31+G(d,p).

included in a continuum of reaction paths, where one extreme is represented by the fully synchronous symmetrical transition structures and the other is represented by the addition, a one-step reaction. Experimental design may modulate the necessary conditions leading from one mechanism to the other, with a polar, ionic medium favoring the addition reaction.

Figure 9 shows the C−C and C−O bond distances in the transition structures leading to the open adduct obtained from the protonated quinone methides in the **27** and **28** approach modes. As can be seen, the two distances are sufficiently different, with the C−C bond distance always being much shorter than the C−O bond distance, justifying the stepwise pathway.

To confirm the formation of the addition adduct in the protonated case, the final geometry obtained in the IRC calculation was optimized. The open adduct (**31**) was obtained, rather than the cycloaddition product, for the **27** and **28** approximation modes. Optimization using water as an implicit solvent starting from the intermediate obtained in the IRC calculation of **29**,exo-TS also afforded addition adduct **31**, although the optimization in the gas phase of the same intermediate resulted in the cycloaddition product. The solvation effect can also contribute to the stabilization of the partial transient negative charge in the transition state for the formation of the open adduct.

To completely reconcile the computational results with the experimental findings, we have to consider the relative stabilities of the starting quinone methides. As discussed before, the *Z* isomer (**15**) is the most stable one (see Table S1). Although isomer interconversion equilibrium is not possible, this should be the preferable isomeric configuration for the quinone methide obtained *in situ* during the reaction of lawsone with the aldehyde. Formation of **15** allows kinetic competition between processes **28** and **29** (Figure 7). The transition structure **28**,endo-TS is preferable to **29**,endo-TS by an energetic difference of 2.64 kcal mol^{-1} (1.73 kcal mol^{-1} in water), affording the open adduct [**31** and **9a** (see Figure 8)]. This would result in the exclusive formation of open adduct **9a**, in agreement with the experimental evidence.

The last step is the cyclization of open adduct **9a** to form the final cyclic xanthenes, which is most easily performed under highly acidic conditions. The protonation of **9a** results in **31** (Figure 10a), and the cyclization of **31** followed by dehydration forms the xanthene derivatives.

A proposed mechanism for the formation of the *ortho-para*-xanthene (**7a**) from **31** is given in Figure 10b. Protonated **31** undergoes intermolecular cyclization by the nucleophilic attack of the deprotonated carboxyl group on the carbon atom containing the hydroxyl group in the protonated naphthoquinone core. Dehydration follows after the protonation of the hydroxyl group and the release of a water molecule, affording the xanthene derivative. A similar mechanism could, of course, also be proposed for the formation of the *ortho-ortho*-xanthene (**8**) derivative. However, the relative Gibbs free energy shows that species **7a** is more stable than **8** by 5.81 kcal mol^{-1}. Therefore, the preferential formation of the *ortho-para* derivative is evident.

DOI: 10.1021/acs.joc.6b00864
J. Org. Chem. 2016, 81, 5525−5537

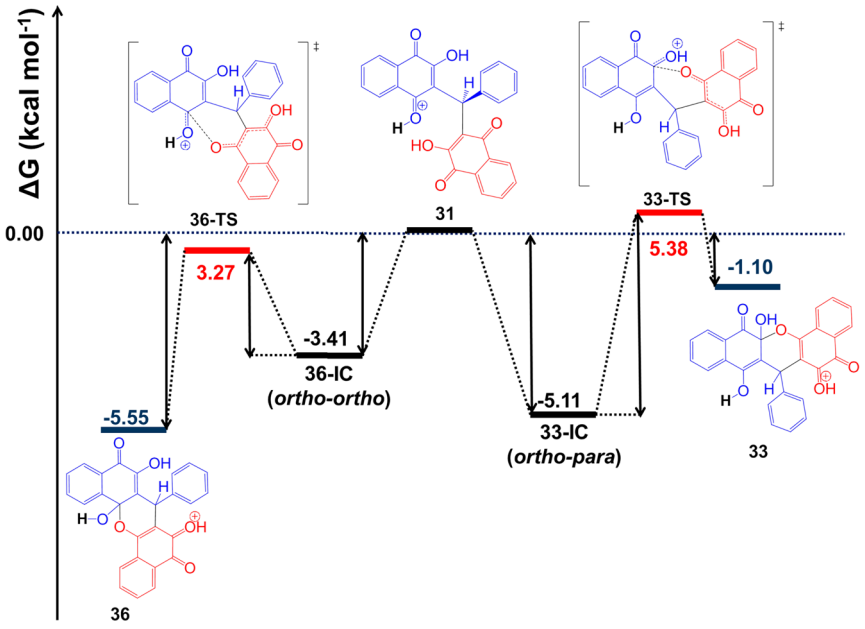

Figure 11. Gibbs free energy change for the cyclization reaction of **31** in the gas phase. All values are in kilocalories per mole. The total Gibbs free energy of structure **31** was taken to be zero. Method: wb97xd/6-31+G(d,p).

The activation energy barriers for the intermolecular cyclization reaction of **31** (Figure 11) and the reverse process range from 1.4 to 5.4 kcal mol^{-1}. With these low activation barriers, the kinetic control is not relevant, and the cyclization proceeds to the most stable products, consistent with the experimental formation of the *ortho-para*-xanthene derivative (**7a**).

CONCLUSION

A new method for the synthesis of 6*H*-dibenzo[*b*,*h*]xanthenes under solvent-free conditions was developed and used to synthesize a series of eight new 6*H*-dibenzo[*b*,*h*]xanthenes (**7a**–**h**) in good yields. This reaction explored *in situ* the generation of *o*-quinone methides via the Knoevenagel condensation between lawsone and appropriate aldehydes followed by nucleophilic addition. The reactions were evaluated under both conventional heating and microwave irradiation, but they worked better under conventional heating conditions. The structure of 6*H*-dibenzo[*b*,*h*]xanthenes **7a** was confirmed by spectroscopic techniques and X-ray crystallography of *o*-phenylenediamine derivative **11a**, which indicated that under these experimental conditions, *ortho-para* isomers were formed.

The reaction mechanism might occur via an open intermediate obtained after the addition reaction between the protonated *Z*-quinone methide and a second lawsone molecule. This protonated species can be present in the reaction mixture due to the protonation/deprotonation equilibrium of the 1,2-quinone moiety during the *in situ* formation of the quinone methide. The calculated energy barrier for the addition process is 10–16 kcal mol^{-1}, lower than for the competitive process that would directly afford the dibenzo[*b*,*h*]xanthene derivative. This stepwise pathway proceeds through a highly asynchronous transition state characterized by highly polar interactions and a low distortion energy. The 6*H*-dibenzo[*b*,*h*]xanthene derivative is formed in a second step by the cyclization/dehydration of the open intermediate, where the higher stability of the *ortho-para* isomer controls the regioselectivity of the reaction.

EXPERIMENTAL SECTION

General Methods. Melting points were measured and are uncorrected. IR spectra were recorded on a spectrophotometer in anhydrous KBr. ^{1}H and ^{13}C NMR spectra were recorded on a 500 MHz spectrophotometer in the solvents indicated using tetramethylsilane (TMS) or the solvent as an internal reference. The chemical shift values (δ) are given in parts per million. Mass spectra were recorded on a high-resolution TOF apparatus, using the technique of "electrospray ionization". The fragments are described as the relation between atomic mass units and the load (m/z).

General Procedure for the Preparation of 6*H*-Dibenzo[*b*,*h*]-xanthene Derivatives (7a–h). A round-bottom flask was charged with lawsone (2 mmol, 348 mg), an appropriate aldehyde (1 mmol), and dry *p*-toluenesulfonic acid (0.6 mmol, 100 mg). The compounds were thoroughly mixed and heated in an oven preheated to 80–100 °C for 6–7 h. At the end of the heating, the solid mixture was poured into 5% aqueous sodium bisulfite and then washed with water. The solid was washed with hot ethanol and hexane to remove impurities.

*7-Phenyl-6H-dibenzo[b,h]xanthene-5,6,8,13(7H)-tetraone (**7a**).* Brick-red solid: yield 79% (330 mg); mp 277–280 °C dec; IR ν_{max} (KBr) 1659, 1590, 1489, 1456, 1361, 1334, 1290, 1230, 1191, 1093, 1014, 977, 944, 911, 844, 802, 774, 720, 699, 670 cm^{-1}; ^{1}H NMR (500 MHz, $CDCl_3$) δ 8.26 (dd, J = 7.8 and 1.0 Hz, 1H), 8.19–8.21 (m, 1H), 8.14 (dd, J = 7.8 and 1.0 Hz, 1H), 8.06–8.04 (m, 1H), 7.83 (dt, J = 7.8 and 1.0 Hz, 1H), 7.79–7.74 (m, 2H), 7.64 (dt, J = 7.8 and 1.0 Hz, 1H), 7.45–746 (m, 2H), 7.25–7.28 (m, 2H), 7.17–7.20 (m, 1H), 5.37 (s, 1H); ^{13}C NMR (125 MHz, $CDCl_3$) δ 182.4, 177.9, 177.4, 177.3, 156.1, 148.5, 140.9, 135.6, 134.7, 134.0, 131.8, 131.6, 130.6, 129.9, 129.8, 129.7, 128.8, 128.7, 127.8, 126.8, 126.6, 125.2, 124.9, 116.1, 33.2; HRESIMS m/z 441.0729 $[M + Na]^+$ (calcd for $C_{27}H_{14}O_5Na^+$ m/z 441.0733).

*7-(4-Bromophenyl)-6H-dibenzo[b,h]xanthene-5,6,8,13(7H)-tetraone (**7b**).* Yellow solid: yield 73% (362 mg); mp 295–296 °C; IR ν_{max} (KBr) 1663, 1610, 1588, 1487, 1355, 1273, 1229, 1197, 1095, 1069, 1010, 975, 946, 834, 771, 715, 672, 639 cm^{-1}; ^{1}H NMR (500 MHz, $CDCl_3$ and CF_3CO_2D) δ 8.30 (d, J = 7.6 Hz, 1H), 8.24–8.26 (m, 1H), 8.08 (d, J = 7.6 Hz, 1H), 8.07–8.09 (m, 1H), 7.91 (dt, J = 7.7 and 1.1 Hz, 1H), 7.83–7.85 (m, 2H), 7.72 (dt, J = 7.7 and 1.1 Hz, 1H), 7.43 (d, J = 8.8 Hz, 2H), 7.32 (d, J = 8.8 Hz, 2H), 5.31 (s, 1H); ^{13}C NMR (125 MHz, $CDCl_3$ and CF_3CO_2D) δ 183.3, 179.1, 178.5, 178.1, 158.4, 148.5, 138.8, 136.7, 135.9, 135.7, 134.8, 134.3, 132.8, 132.7, 132.1, 131.9, 131.2, 130.7, 130.2, 129.3, 127.2, 125.8. 122.3,

DOI: 10.1021/acs.joc.6b00864
J. Org. Chem. 2016, 81, 5525–5537

32.8; HRESIMS m/z 518.9849 $[M + Na]^+$ (calcd for $C_{27}H_{13}BrO_5Na^+$ m/z 518.9838).

*7-(3-Chlorophenyl)-6H-dibenzo[b,h]xanthene-5,6,8,13(7H)-tetraone (**7c**).* Red solid: yield 79% (357 mg); mp 269−273 °C (with small decomposition); IR ν_{max} (KBr) 1661, 1609, 1576, 1477, 1430, 1352, 1294, 1270, 1231, 1195, 1166, 1078, 1009, 949, 896, 854, 794, 757, 726, 683 cm^{-1}; ^1H NMR (500 MHz, $CDCl_3$ and CF_3CO_2D) δ 8.30 (d, J = 7.6 Hz, 1H), 8.22−8.25 (m, 1H), 8.18 (d, J = 7.0 Hz, 1H), 8.06−8.09 (m, 1H), 7.99 (d, J = 8.2 Hz, 1H), 7.90 (dt, J = 7.6, 1.1 Hz, 1H), 7.81−7.84 (m, 1H), 7.71 (d, J = 7.6 Hz, 1H), 7.62−7.68 (m, 1H), 7.46 (d, J = 8.2 Hz, 1H), 7.38−7.42 (m, 1H), 7.18−7.24 (m, 1H), 5.31 (s, 1H); ^{13}C NMR (125 MHz, $CDCl_3$ and CF_3CO_2D) δ 182.8, 178.8, 177.8, 171.5, 158.0, 148.6, 142.1, 136.5, 135.4, 134.9, 134.7, 132.7, 130.6, 130.4, 130.2, 130.1, 129.5, 129.4, 128.6, 128.5, 128.4, 127.4, 127.2, 127.1, 125.9, 115.2, 33.1; HRESIMS m/z 475.0354 $[M + Na]^+$ (calcd for $C_{27}H_{13}ClO_5Na^+$ m/z 475.0343).

*7-(4-Chlorophenyl)-6H-dibenzo[b,h]xanthene-5,6,8,13(7H)-tetraone (**7d**).* Yellow solid: yield 82% (370 mg); mp 259−260 °C (with small decomposition); IR ν_{max} (KBr) 1662, 1609, 1587, 1489, 1408, 1354, 1272, 1228, 1194, 1165, 1090, 1034, 1009, 946, 897, 837, 796, 771, 715, 643 cm^{-1}; ^1H NMR (500 MHz, $CDCl_3$ and CF_3CO_2D) δ 8.29 (d, J = 7.4 Hz, 1H), 8.23−8.25 (m, 1H), 8.18 (d, J = 7.4 Hz, 1H), 8.07−8.08 (m, 1H), 7.90 (dt, J = 7.4, 1.3 Hz, 1H), 7.81−7.55 (m, 2H), 7.71 (dt, J = 7.4, 1.3 Hz, 1H), 7.38 (d, J = 8.7 Hz, 2H), 7.27 (d, J = 8.7 Hz, 2H), 5.32 (s, 1H); ^{13}C NMR (125 MHz, $CDCl_3$ and CF_3CO_2D) δ 185.5, 183.1, 179.1, 178.1, 148.8, 138.9, 136.8, 135.7, 134.9, 134.4, 132.9, 131.6, 130.8, 130.6, 130.3, 129.7, 129.6, 129.4, 127.4, 127.4, 127.4, 126.0, 125.2, 33.0; HRESIMS m/z $[M + Na]^+$ 475.0354 (calcd for $C_{27}H_{13}ClO_5Na^+$ m/z 475.0343).

*7-(Perfluorophenyl)-6H-dibenzo[b,h]xanthene-5,6,8,13(7H)-tetraone (**7e**).* Yellow solid: yield 80% (406 mg); mp 115−116 °C; IR ν_{max} (KBr) 1662, 1612, 1591, 1504, 1359, 1275, 1231, 1195, 1013, 994, 960, 885, 774, 718, 670 cm^{-1}; ^1H NMR (500 MHz, $CDCl_3$ and CF_3CO_2D) δ 8.31 (d, J = 7.8 Hz, 1H), 8.23−8.25 (m, 1H), 8.14 (dd, J = 7.8, 1.5 Hz, 1H), 8.08−8.10 (m, 1H), 7.88 (dt, J = 7.8, 1.5 Hz, 1H), 7.82−7.84 (m, 2H), 7.72 (dt, J = 7.8, 1.5 Hz, 1H), 5.66 (s, 1H); ^{13}C NMR (125 MHz, $CDCl_3$ and CF_3CO_2D) δ 182.8, 178.6, 177.6, 177.2, 159.3, 149.5, 136.6, 135.5, 134.8, 133.0, 131.0, 130.5, 130.2, 130.1, 129.3, 129.0, 128.3, 128.2, 127.2, 127.0, 124.8, 124.1, 120.9, 126.8, 126.0, 111.5, 23.4; HRESIMS m/z 531.0287 (calcd for $C_{27}H_9F_5O_5Na^+$ m/z 531.0262).

*7-(2,4-Dichlorophenyl)-6H-dibenzo[b,h]xanthene-5,6,8,13(7H)-tetraone (**7f**).* Yellow solid: yield 68% (330 mg); mp 243−244 °C; IR ν_{max} (KBr) 1662, 1586, 1471, 1354, 1331, 1289, 1231, 1193, 1162, 1093, 1048, 1012, 975, 946, 848, 814, 762, 716, 665 cm^{-1}; ^1H NMR (500 MHz, $CDCl_3$ and CF_3CO_2D) δ 8.33 (d, J = 7.6 Hz, 1H), 8.24−8.27 (m, 1H), 8.19 (d, J = 7.6 Hz, 1H), 8.06−8.10 (m, 1H), 7.92 (t, J = 7.6 Hz, 1H), 7.84−7.87 (m, 2H), 7.73 (dt, J = 7.6, 1.2 Hz, 1H), 7.53 (d, J = 8.8 Hz, 1H), 7.34 (d, J = 2.3 Hz, 1H), 7.26 (dd, J = 8.8, 2.3 Hz, 1H), 5.60 (s, 1H); ^{13}C NMR (125 MHz, $CDCl_3$ and CF_3CO_2D) δ 183.2, 182.8, 179.1, 177.9, 158.8, 149.2, 136.7, 136.0, 135.6, 135.0, 134.8, 133.9, 132.9, 131.4, 130.9, 130.9, 130.7, 130.5, 130.4, 129.5, 129.4, 128.7, 128.3, 127.7, 127.3, 126.0, 32.7; HRESIMS m/z 508.9968 (calcd for $C_{27}H_{12}Cl_2O_5Na^+$ m/z 508.9954).

*7-(3-Nitrophenyl)-6H-dibenzo[b,h]xanthene-5,6,8,13(7H)-tetraone (**7g**).* Orange solid: yield 72% (333 mg); mp 300−305 °C dec; IR ν_{max} (KBr) 1661, 1589, 1523, 1485, 1348, 1299, 1273, 1229, 1191, 1162, 1094, 1015, 953, 908, 878, 802, 754, 723, 666 cm^{-1}; ^1H NMR (500 MHz, $CDCl_3$ and CF_3CO_2D) δ 8.35 (d, J = 8.0 Hz, 1H), 8.27−8.29 (m, 1H), 8.23 (s, 1H), 8.20 (d, J = 8.0 Hz, 1H), 8.12 (d, J = 8.0 Hz, 2H), 8.06−8.08 (m, 1H), 7.98 (d, J = 8.0 Hz, 1H), 7.95 (t, J = 8.0 Hz, 1H), 7.84−7.88 (m, 2H), 7.75 (t, J = 8.0 Hz, 1H), 5.47 (s, 1H); ^{13}C NMR (125 MHz, $CDCl_3$ and CF_3CO_2D) δ 183.5, 179.4, 178.5, 178.3, 159.1, 149.3, 148.6, 142.7, 137.2, 136.5, 136.1, 135.4, 133.4, 131.5, 131.1, 130.6, 130.3, 129.6, 129.5, 127.7, 127.6, 126.5, 124.5, 123.7, 123.7, 114.7, 33.8; HRESIMS m/z 486.0579 $[M + Na]^+$ (calcd for $C_{27}H_{13}NO_7Na^+$ m/z 486.0584).

*7-o-Tolyl-6H-dibenzo[b,h]xanthene-5,6,8,13(7H)-tetraone (**7h**).* Orange solid: yield 72% (311 mg); mp 304−306 °C (with small decomposition); IR ν_{max} (KBr) 1671, 1606, 1519, 1480, 1343, 1259, 1212, 1094, 1041, 989, 859, 792, 719 cm^{-1}; ^1H NMR (500 MHz, $CDCl_3$ and CF_3CO_2D) δ 8.26 (d, J = 7.8 Hz, 1H), 8.16−8.18 (m, 1H), 8.06 (d, J = 7.8 Hz, 1H), 7.97−8.00 (m, 1H), 7.84 (dt, J = 7.8, 1.0 Hz, 1H), 7.71−7.84 (m, 3H), 7.63−7.66 (m, 2H), 7.48 (dd, J = 7.8 2.0 Hz, 1H), 7.29 (d, J = 7.8 Hz, 1H), 5.45 (s, 1H), 2.96 (s, 3H, CH_3); ^{13}C NMR (125 MHz, $CDCl_3$ and CF_3CO_2D) δ 183.4, 181.2, 179.5, 178.1, 158.7, 149.0, 141.1, 136.8, 136.0, 135.6, 134.8, 134.1, 132.9, 131.7, 131.5, 130.6, 130.4, 129.6, 129.3, 127.5, 127.3, 127.2, 127.0, 126.2, 125.5, 125.1, 30.6, 20.1; HRESIMS m/z 455.0880 $[M + Na]^+$ (calcd for $C_{28}H_{16}O_5Na^+$ m/z 455.0890).

General Procedure for the Preparation of 3,3′-(Phenylmethylene)bis(2-hydroxynaphthalene-1,4-dione) (9a). A 50 mL solution of lawsone (2 mmol) and benzaldehyde (1 mmol) in EtOH/H_2O solvent [1:1 (v/v)] was refluxed for 12 h. The solid that formed was filtered, and the precipitate was washed with water and then EtOH. The solid was stored in a desiccator with phosphorus pentoxide to remove residual water to afford pure product **9a**: yellow solid; yield 83% (361 mg); mp 201−202 °C (lit. 202−204 °C); IR ν_{max} (KBr) 3335, 1641, 1591, 1496, 1459, 1326, 1299, 1275, 1158, 1080, 1039, 1020, 972, 896, 866, 791, 767, 722, 650 cm^{-1}; ^1H NMR (500 MHz, $CDCl_3$) δ 8.18 (bs, 1H), 8.10 (d, J = 7.3 Hz, 2H), 8.09 (d, J = 7.3 Hz, 2H), 7.75 (t, J = 7.3 Hz, 2H), 7.69 (t, J = 7.3 Hz, 2H), 7.33−7.19 (m, 5H, Ph), 6.25 (s, 1H, H-3); ^{13}C NMR (125 MHz, $CDCl_3$) δ 37.5, 122.5, 126.3, 126.7, 127.2, 128.0, 128.3, 129.5, 132.6, 133.2, 135.0, 137.8, 154.8, 181.2, 184.7; HRESIMS m/z 459.0835 $[M + Na]^+$ (calcd for $C_{27}H_{16}O_6Na^+$ m/z 459.0839).

General Procedure for the Preparation of 3,3′-(Phenylmethylene)bis(2-methoxynaphthalene-1,4-dione) (10a). A 30 mL solution of **9a** (0.48 mmol), dimethyl sulfate (0.49 mmol), and potassium carbonate (0.49 mmol) in acetone was refluxed for 6 h. The potassium carbonate was removed by filtration and by the evaporation of acetone to afford product **10a**: brown solid; yield 60% (133 mg); mp 110 °C dec; IR ν_{max} (KBr) 1670, 1591, 1516, 1343, 1294, 195, 1109, 1048, 978, 855, 787, 717 cm^{-1}; ^1H NMR (500 MHz, $CDCl_3$ and CF_3CO_2D) δ 8.02 (d, J = 5.4 Hz, 2H), 8.01 (t, J = 5.4 Hz, 2H), 7.68−7.66 (m, 4H), 7.26−7.25 (m, 5H), 6.04 (s, 1H), 3.70 (s, 6H); ^{13}C NMR (125 MHz, $CDCl_3$) δ 40.0, 58.5, 126.0, 126.3, 126.6, 128.1, 128.2, 128.4, 131.4, 132.0, 133.3, 133.9, 135.2, 158.2, 181.9, 184.7; HRESIMS m/z 487.1152 $[M + Na]^+$ (calcd for $C_{29}H_{20}O_6Na^+$ m/z 487.1134).

General Procedure for the Preparation of 17-Phenyl-11*H*-benzo[*a*]benzo[6,7]chromeno[2,3-*c*]phenazine-11,16(17*H*)-dione (11a). A mixture of **7a** (1 mmol), *o*-phenylenediamine (2.3 mmol), and sodium acetate (7.9 mmol) was solubilized in glacial acetic acid (5 mL). The mixture was stirred overnight at room temperature and then poured into cold water (25 mL). The precipitate was filtered and washed in water until neutrality was reached to afford product **11a**:[73] orange solid; yield 76% (372 mg); mp 328−331 °C dec; IR ν_{max} (KBr) 1681, 1590, 1529, 1495, 1449, 1409, 1352, 1260, 1232, 1085, 1061, 1032, 986, 952, 799, 758, 729, 698 cm^{-1}; ^1H NMR (500 MHz, $CDCl_3$) δ 8.32 (d, J = 7.3 Hz, 1H), 8.26−8.25 (m, 1H), 8.16 (d, J = 7.3 Hz, 1H), 8.13−8.03 (m, 2H), 7.91 (t, J = 7.3 Hz, 2H), 7.84−7.77 (m, 3H), 7.71 (t, J = 7.3 Hz, 2H), 7.55 (dd, J = 7.3, 1.3 Hz, 1H), 7.32−7.16 (m, 4H), 5.62 (s, 1H); ^{13}C NMR (125 MHz, $CDCl_3$ and CF_3CO_2D) δ 183.8, 179.4, 178.4, 178.3, 159.1, 149.3, 137.0, 136.7, 136.1, 135.8, 135.0, 134.3, 134.2, 133.1, 133.0, 131.6, 130.9, 130.8, 130.5, 129.8, 129.7, 129.6, 127.8, 127.5, 127.4, 127.1, 126.2, 123.9, 121.7, 114.3, 33.1. HRESIMS m/z 491.1380 $[M + H]^+$ (calcd for $C_{33}H_{19}N_2O_3^+$ m/z 491.1390).

X-ray Crystal Structure of 11a. A single crystal of derivative **11a** was selected for crystallographic analysis. X-ray diffraction data were collected at 150 K using monochromatic Mo Kα radiation on a Bruker D8 Venture diffractometer system with a CMOS Photon 100 detector. Intensities were collected with ω and ϕ scans and were corrected for Lorentz and polarization effects with APEX2 suite. An empirical absorption correction (multiscan) was also applied to all measured intensities using the SADABS program. The structures were determined by direct methods and refined by full-matrix least squares on F^2 using a combination of the SHELX-2013 package[74] and Olex2 software.[75] All non-hydrogen atoms were refined with anisotropic

DOI: 10.1021/acs.joc.6b00864
J. Org. Chem. 2016, 81, 5525−5537

displacement parameters. Hydrogen atoms bonded to C atoms were placed at their idealized positions using standard geometric criteria. Crystallographic data for **11a**: $C_{33}H_{18}N_2O_3$, FW 490.49, colorless block (crystal dimensions of 0.122 mm × 0.251 mm × 0.431 mm), monoclinic, space group $P\bar{1}$, a = 10.6689(4) Å, b = 10.9978(5) Å, c = 11.8961(6) Å, α = 81.299(2)°, β = 66.4970(10)°, γ = 62.7020(10)°, volume of 1136.62(9) Å^3, Z = 2, D_c = 1.43 g/cm^3, μ = 0.093 mm^{-1}, $F(000)$ = 508. A total of 31178 reflections were measured, of which 4323 were independent. R_{int} = 0.0397. Data set $-12 \le h \le 13$, $-13 \le k \le 13$, $-14 \le l \le 14$. The final anisotropic full-matrix least-squares refinement on F^2 with 343 variables converged at R1 = 3.86% for the observed data and R2 = 10.88% for all data. CCDC number 1415612.

Computational Methods. To shed some light on the possible mechanism for this reaction, we performed a set of computational studies for the most relevant steps. Full geometry optimizations were conducted in the gas phase using the wb97xd[76] functional together with the 6-31+G(d,p) basis set.[77,78] The default Gaussian convergence criterion was employed. For each optimized stationary point, the second-order Hessian matrix was computed at the same level to confirm the stationary point as a minimum, a geometry with all eigenvalues positive, or a transition structure, with just one negative eigenvalue of the Hessian matrix. For each transition structure, the negative normal mode was animated to confirm that it connects the desired minima. Additionally, an intrinsic reaction coordinate (IRC) calculation,[79−81] starting from the transition structure, was conducted to confirm that the forward and backward reactions passing through that transition structure connect the reactants to the products and vice versa. The final points obtained from the IRC calculations were employed as initial geometries for the optimization and energy calculation of the local minima. The normal mode calculations were also useful for computing the thermodynamic parameters at 298 K using standard statistical thermodynamic equations. All relative energy values are given as the Gibbs free energy (ΔG^{298}), computed using unscaled frequencies.

Solvation effects were accounted for during the optimization by using water as an implicit solvent in the polarized continuum solvation model (IEFPCM).[82,83] All computations were performed with the G09 software package.[84]

■ ASSOCIATED CONTENT

Supporting Information

The Supporting Information is available free of charge on the ACS Publications website at DOI: 10.1021/acs.joc.6b00864.

IR, HRMS, ^{1}H NMR, and ^{13}C NMR spectra for all new products (PDF)

Copies of crystal structure determinations (CIF)

■ AUTHOR INFORMATION

Corresponding Author

*E-mail: cegvito@vm.uff.br.

Notes

The authors declare no competing financial interest.

■ ACKNOWLEDGMENTS

The authors are grateful to the CAPES, CNPq, and FAPERJ for funding this research project. The authors also thank LaReMN/UFF and LARE-DRX/UFF (FAPERJ) for the NMR and X-ray data.

■ REFERENCES

(1) Moosophon, P.; Kanokmedhakul, S.; Kanokmedhakul, K.; Soytong, K. *J. Nat. Prod.* **2009**, *72*, 1442.

(2) Hay, A. E.; Aumond, M. C.; Mallet, S.; Dumontet, V.; Litaudon, M.; Rondeau, D.; Richomme, P. *J. Nat. Prod.* **2004**, *67*, 707.

(3) Hashim, N.; Rahmani, M.; Sukari, M. A.; Ali, A. M.; Alitheen, N. B.; Go, R.; Ismail, H. B. M. *J. Asian Nat. Prod. Res.* **2010**, *12*, 106.

(4) Li, X.; Zhang, H.; Xie, Y.; Hu, Y.; Sun, H.; Zhu, Q. *Org. Biomol. Chem.* **2014**, *12*, 2033.

(5) Chibale, K.; Visser, M.; van Schalkwyk, D.; Smith, P. J.; Saravanamuthu, A.; Fairlamb, A. H. *Tetrahedron* **2003**, *59*, 2289.

(6) Jamison, J. M.; Krabill, K.; Hatwalkar, A.; Jamison, E.; Tsai, C. C. *Cell Biol. Int. Rep.* **1990**, *14*, 1075.

(7) Evangelinou, O.; Hatzidimitriou, A. G.; Velali, E.; Pantazaki, A. A.; Voulgarakis, N.; Aslanidis, P. *Polyhedron* **2014**, *72*, 122.

(8) Yunnikova, L. P.; Gorokhov, V. Yu.; Makhova, T. V.; Aleksandrova, G. A. *Pharm. Chem. J.* **2013**, *47*, 139.

(9) Azebaze, A. G.; Meyer, M.; Valentin, A.; Nguemfo, E. L.; Fomum, Z. T.; Nkengfack, A. E. *Chem. Pharm. Bull.* **2006**, *54*, 111.

(10) Zelefack, F.; Guilet, D.; Fabre, N.; Bayet, C.; Chevalley, S. V.; Ngouela, S.; Lenta, B. N.; Valentin, A.; Tsamo, E.; Dijoux-Franca, M.-G. *J. Nat. Prod.* **2009**, *72*, 954.

(11) Laphookhieo, S.; Syers, J. K.; Kiattansakul, R.; Chantrapromma, K. *Chem. Pharm. Bull.* **2006**, *54*, 745.

(12) Djoufack, G. L.; Valant-Vetschera, K. M.; Schinnerl, J.; Brecker, L.; Lorbeer, E.; Robien, W. *Nat. Prod. Commun.* **2010**, *5*, 1055.

(13) Poupelin, J. P.; Saint-Ruf, G.; Foussard-Blanpin, O.; Marcisse, G.; Uchida-Ernouf, G.; Lacroix, R. *Eur. J. Med. Chem.* **1978**, *13*, 67.

(14) Rewcastle, G. W.; Atwell, G. J.; Zhuang, L.; Baguley, B. C.; Denny, W. A. *J. Med. Chem.* **1991**, *34*, 217.

(15) Niu, S. L.; Li, Z. L.; Ji, F.; Liu, G. Y.; Zhao, N.; Liu, X. Q.; Jing, Y. K.; Hua, H. M. *Phytochemistry* **2012**, *77*, 280.

(16) Lee, K. H.; Chai, H. B.; Tamez, P. A.; Pezzuto, J. M.; Cordell, G. A.; Win, K. K.; Tin-Wa, M. *Phytochemistry* **2003**, *64*, 535.

(17) Tao, S. J.; Guan, S. H.; Wang, W.; Lu, Z. Q.; Chen, G. T.; Sha, N.; Yue, Q. X.; Liu, X.; Guo, D. A. *J. Nat. Prod.* **2009**, *72*, 117.

(18) Diniz, T. F.; Pereira, A. C.; Capettini, L. S. A.; Santos, M. H.; Nagem, T. J.; Lemos, V. S.; Cortes, S. F. *Planta Med.* **2013**, *79*, 1495.

(19) Ion, R. M.; Planner, A.; Wiktorowicz, K.; Frackowiak, D. *Acta Biochim. Polym.* **1998**, *45*, 833.

(20) Jha, A.; Beal, J. *Tetrahedron Lett.* **2004**, *45*, 8999.

(21) Knight, D. W.; Little, P. B. *J. Chem. Soc. Perkin Trans. 1* **2001**, 1771.

(22) Knight, D. W.; Little, P. B. *Synlett* **1998**, *1998*, 1141.

(23) Pasha, M. A.; Jayashankara, V. P. *Bioorg. Med. Chem. Lett.* **2007**, *17*, 621.

(24) de Carvalho da Silva, F. C.; Francisco Ferreira, V. F. *Curr. Org. Synth.* **2016**, *13*, 334.

(25) Salmon-Chemin, L.; Buisine, E.; Yardley, V.; Kohler, S.; Debreu, M. A.; Landry, V.; Sergheraert, C.; Croft, S. L.; Krauth-Siegel, R. L.; Davioud-Charvet, E. *J. Med. Chem.* **2001**, *44*, 548.

(26) Müller, T.; Johann, L.; Jannack, B.; Brückner, M.; Lanfranchi, D. A.; Bauer, H.; Sanchez, C.; Yardley, V.; Deregnaucourt, C.; Schrevel, J.; Lanzer, M.; Schirmer, R. H.; Davioud-Charvet, E. *J. Am. Chem. Soc.* **2011**, *133*, 11557.

(27) dos Santos, E. V. M; Carneiro, J. W. M.; Ferreira, V. F. *Bioorg. Med. Chem.* **2004**, *12*, 87.

(28) Hickman, J. A. *Curr. Opin. Genet. Dev.* **2002**, *12*, 67.

(29) Zani, C. L.; Chiari, E.; Krettli, A. U.; Murta, S. M. F.; Cunningham, M. L.; Fairlamb, A. H.; Romanha, A. J. *Bioorg. Med. Chem.* **1997**, *5*, 2185.

(30) Villamil, S. F.; Stoppani, A. O. M.; Dubin, M. *Methods Enzymol.* **2004**, *378*, 67.

(31) Benites, J.; Valderrama, J. A.; Rivera, F.; Rojo, L.; Campos, N.; Pedro, M.; José Nascimento, M. S. J. *Bioorg. Med. Chem.* **2008**, *16*, 862.

(32) Silva, M. N.; de Souza, M. C. B. V.; Ferreira, V. F.; Pinto, A. V.; Goulart, M. C. R. F.; Wardell, S. M. V.; Wardell, J. L. *Arkivoc* **2003**, 156.

(33) Cao, Y.; Yao, C.; Qin, B.; Zhang, H. *Res. Chem. Intermed.* **2013**, *39*, 3055.

(34) Das, B.; Ravikanth, B.; Ramu, R.; Laxminarayana, K.; Rao, B. V. *J. Mol. Catal. A: Chem.* **2006**, *255*, 74.

(35) Yadav, S.; Nand, B.; Khurana, J. M. *Can. J. Chem.* **2013**, *91*, 698.

(36) Soleimani, E.; Khodaei, M. M.; Taheri Kal Koshvandi, A. *Chin. Chem. Lett.* **2011**, *22*, 927.

DOI: 10.1021/acs.joc.6b00864
J. Org. Chem. 2016, 81, 5525−5537

(37) Wu, L. Q.; Wu, Y. F.; Yang, C. G.; Yang, L. M.; Yang, L. J. *J. Braz. Chem. Soc.* **2010**, *21*, 941.
(38) Safaei-Ghomi, J.; Ghasemzadeh, M. A. *S. Afr. J. Chem.* **2014**, *67*, 27.
(39) Zang, H.; Zhang, Y.; Cheng, B.; Zhang, W.; Xu, X.; Ren, Y. *Chin. J. Chem.* **2012**, *30*, 362.
(40) Singh, H.; Kumari, S.; Khurana, J. M. *Chin. Chem. Lett.* **2014**, *25*, 1336.
(41) Huo, C.-D.; Bao, X.-Z.; Hu, D.-C.; Jia, X.-D.; Sun, C.-G.; Wang, C. *Chin. Chem. Lett.* **2014**, *25*, 699.
(42) Wu, L.; Zhang, J.; Fang, L.; Yang, C.; Yan, F. *Dyes Pigm.* **2010**, *86*, 93.
(43) Kantevari, S.; Chary, M. V.; Rudra Das, A. P.; Vuppalapati, S. V. N.; Lingaiah, N. *Catal. Commun.* **2008**, *9*, 1575.
(44) Rahmati, A. *Chin. Chem. Lett.* **2010**, *21*, 761.
(45) Chen, Y.; Wu, S.; Tu, S.; Li, C.; Shi, F. *J. Heterocycl. Chem.* **2008**, *45*, 931.
(46) Wu, L.; Wu, Y.; Yan, F.; Fang, L. *Monatsh. Chem.* **2010**, *141*, 871.
(47) Yang, X.; Yang, L.; Wu, L. *Bull. Korean Chem. Soc.* **2013**, *34*, 1303.
(48) Rahmatpour, A. *Monatsh. Chem.* **2013**, *144*, 1205.
(49) Du, B.; Cai, G.; Zhao, B.; Meng, X.; Wang, X.; Li, Y. *Res. Chem. Intermed.* **2013**, *39*, 1323.
(50) Khurana, J. M.; Lumb, A.; Chaudhary, A.; Nand, B. *Synth. Commun.* **2013**, *43*, 2147.
(51) Olyaei, A.; Alidoust, M. G. *Synth. Commun.* **2015**, *45*, 94.
(52) Dabiri, M.; Tisseh, Z. N.; Bazgir, A. *J. Heterocycl. Chem.* **2010**, *47*, 1062.
(53) Tisseh, Z. N.; Azimi, S. C.; Mirzaei, P.; Bazgir, A. *Dyes Pigm.* **2008**, *79*, 273.
(54) Tavakoli, H. R.; Moosavi, S. M.; Bazgir, A. *Res. Chem. Intermed.* **2015**, *41*, 3041.
(55) Chen, Y.; Wu, S.; Tu, S.; Li, C.; Shi, F. *J. Heterocycl. Chem.* **2008**, *45*, 931.
(56) Shaterian, H. R.; Azizi, K.; Fahimi, N. *Res. Chem. Intermed.* **2014**, *40*, 1403.
(57) Shaterian, H. R.; Rigi, F. *Res. Chem. Intermed.* **2015**, *41*, 721.
(58) Amini, M. M.; Fazaeli, Y.; Yassaee, Z.; Feizi, S.; Bazgir, A. *Open Catal. J.* **2009**, *2*, 40.
(59) Khaligh, N. G. *Catal. Sci. Technol.* **2012**, *2*, 2211.
(60) Liu, D.; Gao, J.; Li, L.; Zhou, S.; Xu, D. *Chem. Heterocycl. Compd.* **2013**, *49*, 1370.
(61) Shaterian, H. R.; Sedghipour, M.; Mollashahi, E. *Res. Chem. Intermed.* **2014**, *40*, 1345.
(62) Bazgir, A.; Tisseh, Z. N.; Mirzaei, P. *Tetrahedron Lett.* **2008**, *49*, 5165.
(63) Padmanabha Rao, T. V. P.; Venkateswarlu, V. *Tetrahedron* **1964**, *20*, 2967.
(64) Mathieson, J. W.; Thomson, R. H. *J. Chem. Soc. C* **1971**, 153.
(65) Jordão, A. K.; Vargas, M. D.; Pinto, A. C.; da Silva, F. C.; Ferreira, V. F. *RSC Adv.* **2015**, *5*, 67909.
(66) Tisseh, Z. N.; Bazgir, A. *Dyes Pigm.* **2009**, *83*, 258.
(67) Ferreira, S. B.; da Silva, F. C.; Pinto, A. C.; Gonzaga, D. T. G.; Ferreira, V. F. *J. Heterocycl. Chem.* **2009**, *46*, 1080.
(68) Willis, N. J.; Bray, C. D. *Chem. - Eur. J.* **2012**, *18*, 9160.
(69) Sustmann, R.; Sicking, W. *J. Am. Chem. Soc.* **1996**, *118*, 12562.
(70) Domingo, L. R.; Sáez, J. A. *Org. Biomol. Chem.* **2009**, *7*, 3576.
(71) Sarotti, A. M. *Org. Biomol. Chem.* **2014**, *12*, 187.
(72) Sustmann, R.; Tappanchai, S.; Bandmann, H. *J. Am. Chem. Soc.* **1996**, *118*, 12555.
(73) Hooker, S. *J. Am. Chem. Soc.* **1936**, *58*, 1168.
(74) Sheldrick, G. M. *Acta Crystallogr., Sect. A: Found. Crystallogr.* **2008**, *64*, 112.
(75) Dolomanov, O. V.; Bourhis, L. J.; Gildea, R. J.; Howard, J. A. K.; Puschmann, H. *J. Appl. Crystallogr.* **2009**, *42*, 339.
(76) Chai, J.-D; Head-Gordon, M. *Phys. Chem. Chem. Phys.* **2008**, *10*, 6615.
(77) Francl, M. M.; Pietro, W. J.; Hehre, W. J.; Binkley, J. S.; Gordon, M. S.; DeFrees, D. J.; Pople, J. A. *J. Chem. Phys.* **1982**, *77*, 3654.
(78) Hariharan, P. C.; Pople, J. A. *Chem. Phys. Lett.* **1972**, *16*, 217.
(79) Fukui, K. J. *J. Phys. Chem.* **1970**, *74*, 4161.
(80) Fukui, K. *Acc. Chem. Res.* **1981**, *14*, 363.
(81) Garrett, B. C.; Redmon, M. J.; Steckler, R.; Truhlar, D. G.; Baldridge, K. K.; Bartol, D.; Schmidt, M. W.; Gordon, M. S. *J. Phys. Chem.* **1988**, *92*, 1476.
(82) Mennucci, B.; Cances, E.; Tomasi, J. *J. Phys. Chem. B* **1997**, *101*, 10506.
(83) Tomasi, J.; Mennucci, B.; Cances, E. *J. Mol. Struct.: THEOCHEM* **1999**, *464*, 211.
(84) Frisch, M. J.; Trucks, G. W.; Schlegel, H. B.; Scuseria, G. E.; Robb, M. A.; Cheeseman, J. R.; Scalmani, G.; Barone, V.; Mennucci, B.; Petersson, G. A.; Nakatsuji, H.; Caricato, M.; Li, X.; Hratchian, H. P.; Izmaylov, A. F.; Bloino, J.; Zheng, G.; Sonnenberg, J. L.; Hada, M.; Ehara, M.; Toyota, K.; Fukuda, R.; Hasegawa, J.; Ishida, M.; Nakajima, T.; Honda, Y.; Kitao, O.; Nakai, H.; Vreven, T.; Montgomery, J. A., Jr.; Peralta, J. E.; Ogliaro, F.; Bearpark, M.; Heyd, J. J.; Brothers, E.; Kudin, K. N.; Staroverov, V. N.; Keith, T.; Kobayashi, R.; Normand, J.; Raghavachari, K.; Rendell, A.; Burant, J. C.; Iyengar, S. S.; Tomasi, J.; Cossi, M.; Rega, N.; Millam, J. M.; Klene, M.; Knox, J. E.; Cross, J. B.; Bakken, V.; Adamo, C.; Jaramillo, J.; Gomperts, R.; Stratmann, R. E.; Yazyev, O.; Austin, A. J.; Cammi, R.; Pomelli, C.; Ochterski, J. W.; Martin, R. L.; Morokuma, K.; Zakrzewski, V. G.; Voth, G. A.; Salvador, P.; Dannenberg, J. J.; Dapprich, S.; Daniels, A. D.; Farkas, O.; Foresman, J. B.; Ortiz, J. V.; Cioslowski, J.; Fox, D. J. *Gaussian 09*, revision D.01; Gaussian, Inc.: Wallingford, CT, 2013.

DOI: 10.1021/acs.joc.6b00864
J. Org. Chem. 2016, 81, 5525−5537